J Comput Neurosci
DOI 10.1007/s10827-011-0368-2

Influences of membrane properties on phase response curve and synchronization stability in a model globus pallidus neuron

Tomohiro Fujita · Tomoki Fukai · Katsunori Kitano

Received: 28 April 2011 / Revised: 19 September 2011 / Accepted: 30 September 2011

Abstract The activity patterns of the globus pallidus (GPe) and subthalamic nucleus (STN) are closely associated with motor function and dysfunction in the basal ganglia. In the pathological state caused by dopamine depletion, the STN–GPe network exhibits rhythmic synchronous activity accompanied by rebound bursts in the STN. Therefore, the mechanism of activity transition is a key to understand basal ganglia functions. As synchronization in GPe neurons could induce pathological STN rebound bursts, it is important to study how synchrony is generated in the GPe. To clarify this issue, we applied the phase-reduction technique to a conductance-based GPe neuronal model in order to derive the phase response curve (PRC) and interaction function between coupled GPe neurons. Using the PRC and interaction function, we studied how the steady-state activity of the GPe network depends on intrinsic membrane properties, varying ionic conductances on the membrane. We noted that a change in persistent sodium current, fast delayed rectifier Kv3 potassium current, M-type potassium current and small conductance calcium-dependent potassium current influenced the PRC shape and the steady state. The effect of those currents on the PRC shape could be attributed to extension of the firing period and reduction of the phase response immediately after an action potential. In particular, the slow potassium current arising from the M-type potassium and the SK current was responsible for the reduction of the phase response. These results suggest that the membrane property modulation controls synchronization/asynchronization in the GPe and the pathological pattern of STN–GPe activity.

Keywords Globus pallidus · Synchronization · Phase response curve · Membrane property modulation

Action Editor: Brent Doiron

T. Fujita
Graduate School of Science and Engineering,
Ritsumeikan University,
Kusatsu, Shiga 525-8577, Japan

T. Fukai
Laboratory for Neural Circuit Theory,
RIKEN Brain Science Institute,
Wako, Saitama 351-0198, Japan

K. Kitano (✉)
Department of Human and Computer Intelligence,
Ritsumeikan University,
1-1-1 Nojihigashi,
Kusatsu, Shiga 525-8577, Japan
e-mail: kitano@ci.ritsumei.ac.jp

1 Introduction

The external segment of the globus pallidus (GPe) and subthalamic nucleus (STN) comprise reciprocally connected nuclei and their neuronal activity is considered to modulate the other parts of the basal ganglia (Plenz and Kitai 1999; Bolam et al. 2000; Terman et al. 2002). The evidence that the activity pattern of these nuclei is closely related to motor function and dysfunction suggests that the STN–GPe network plays an important role in basal ganglia functions (DeLong et al. 1985; Bevan et al. 2006; Rivlin-Etzion et al. 2006). Nuclei of the STN–GPe network exhibit tonic desynchronized activity in the normal state, but their rhythmic synchronous activity is accompanied by rebound bursts in the STN in the parkinsonian state caused by dopamine depletion (Magill et al. 2000; Raz et al. 2000; Brown et al. 2001). To induce the rebound bursts of STN neurons, strong inhibitory input to activate low voltage-activated calcium channels on STN neuronal membranes is required (Bevan et al. 2000; Hallworth and Bevan 2005). A

Published online: 13 October 2011

potential source of such inhibition is the synchronization of GPe neurons, which are the major neurons sending GABAergic synaptic input to STN neurons (Bevan et al. 2000; Hallworth and Bevan 2005). Therefore, to understand the mechanism of transition from the normal state to the pathological state, it is important to clarify what determines synchronized and desynchronized activity in GPe neurons and how it is relevant to dopaminergic modulation.

A study of a computational STN–GPe model revealed that reciprocal interaction between the nuclei has a crucial impact on the firing patterns (Terman et al. 2002). Cellular plasticity, presumably caused by dopaminergic modulation, could be a trigger of the firing pattern transition as well. As GPe neurons are driven by GABAergic axonal collaterals as well as excitatory synapses from the STN and GABAergic synapses from the striatum (Kita and Kitai 1994; Sadek et al. 2007), interaction within the GPe could cause entrainment depending on the intrinsic membrane properties. In general, the behavior of a mutually connected network depends on the dynamic property of each unit and the interaction between units. If a unit shows oscillatory activity, the dynamic property is characterized by a phase response curve (PRC) describing to what degree the state of the unit (phase) is advanced or delayed in the cycle by an external perturbation and how the phase advance or delay depends on the timing of the perturbation (Ermentrout and Kopell 1984; Kuramoto 1984). If a PRC consists of both positive and negative components, called type II PRC, the units potentially synchronize in the network. A study of a multicompartmental GPe neuronal model showed a type II PRC at the distal dendrites and suggested that the dendritic PRC contributes to synchronization in the GPe network (Schultheiss et al. 2010).

To elucidate how the dynamic state of the GPe network depends on the intrinsic membrane properties, we derived PRC of a conductance-based model of a GPe neuron proposed by Günay et al. (2008). Using the PRC and dynamic equations of coupled phase oscillators derived with the phase-reduction technique, we studied the steady-state activity of a GPe network connected with GABAergic synapses. Furthermore, we explored how the ionic channels characterizing the membrane properties of our model GPe neuron contributed to the PRC and consequently to the steady-state activity in order to discuss the possibility of membrane property modulation by dopamine to induce steady-state transition in the GPe network.

2 Methods

2.1 Neuronal model

We used a model of a GPe neuron proposed by Günay et al. (2008) but modified it as a single compartment model. The dynamics of membrane potential V can be described by the Hodgkin–Huxley formalism as follows:

$$C_{\mathrm{m}}\frac{dV}{dt} = -g_{\mathrm{leak}}(V-E_{\mathrm{leak}}) + I_{\mathrm{syn}} + I_{\mathrm{app}} - I_{\mathrm{NaF}} - I_{\mathrm{NaP}} - I_{\mathrm{Kv2}} - I_{\mathrm{Kv3}} - I_{\mathrm{Kv4f}} - I_{\mathrm{Kv4s}} - I_{\mathrm{KCNQ}} - I_{\mathrm{CaH}} - I_{\mathrm{HCN}} - I_{\mathrm{SK}},$$

where C_{m} is the unit capacitance (= 1 μF/cm^2). I_{syn} and I_{app} are the synaptic current and external input current, respectively. I_{NaF} and I_{NaP} are the fast transient sodium current and the persistent sodium current, respectively. I_{Kv2}, I_{Kv3}, and I_{Kv4} are the slow delayed rectifier potassium current, fast delayed rectifier potassium current, and A-type transient potassium current, respectively. I_{KCNQ} is the M-type potassium current. I_{CaH} comprises high-voltage-activated calcium currents, including L, N, and P/Q-type channels. I_{HCN} is the hyperpolarization-activated cyclic nucleotide-modulated cation current. I_{SK} is the calcium-dependent potassium current. The various currents are represented by the following equations:

$$\begin{aligned}
I_{\mathrm{NaF}} &= g_{\mathrm{NaF}} m^3 hs(V-E_{\mathrm{Na}}) \\
I_{\mathrm{NaP}} &= g_{\mathrm{NaP}} m^3 hs(V-E_{\mathrm{Na}}) \\
I_{\mathrm{Kv2}} &= g_{\mathrm{Kv2}} m^4 h(V-E_{\mathrm{K}}) \\
I_{\mathrm{Kv3}} &= g_{\mathrm{Kv3}} m^4 h(V-E_{\mathrm{K}}) \\
I_{\mathrm{Kv4f}} &= g_{\mathrm{Kv4f}} m^4 h(V-E_{\mathrm{K}}) \\
I_{\mathrm{Kv4s}} &= g_{\mathrm{Kv4s}} m^4 h(V-E_{\mathrm{K}}) \\
I_{\mathrm{KCNQ}} &= g_{\mathrm{KCNQ}} m^4 (V-E_{\mathrm{K}}) \\
I_{\mathrm{CaH}} &= g_{\mathrm{CaH}} m(V-E_{\mathrm{Ca}}) \\
I_{\mathrm{HCN}} &= g_{\mathrm{HCN}} m(V-E_{\mathrm{cat}}) \\
I_{\mathrm{SK}} &= g_{\mathrm{SK}} m(V-E_{\mathrm{K}}),
\end{aligned}$$

where g_{NaF}, g_{NaP}, g_{Kv2}, g_{Kv3}, g_{Kv4f}, g_{Kv4s}, g_{KCNQ}, g_{CaH}, g_{HCN}, g_{SK}, and g_{leak} are the maximal conductances, and E_{Na}, E_{K}, E_{cat}, E_{Ca}, and E_{leak} are the reversal potentials of sodium, potassium, cation, calcium, and leak current, respectively; m, h, and s are the activation or inactivation variables. As conductances of the ionic currents, except for the Kv3 current, base values in the previous model were used (Günay et al. 2008). The conductance of the Kv3 current was increased from the base value and the base values, not but the suggested values for some somatic conductances, were used here so as to exhibit an autonomous activity that is typically observed in the major type of GPe neurons—the type II (Nambu and Llinás 1994) or the type A (Cooper and Stanford 2000; Stanford 2003). The previous model suggests that somatic conductances of NaF, NaP and SK currents are different from the base values. For the sodium channels, however, the suggested values that are 0.7 times the base values yielded an autonomous activity at a relatively low firing rate (~4 spikes/s) although those did not seem to cause any other qualitative differences. Furthermore, the suggested

SK conductance, which is 16 times as large as the base value, brought so large a SK current that the neuron discharged rhythmic multiplet spikes rather than singlet spikes. This discrepancy between the previous multi-compartment model and the present single compartment model is presumably because of existence/absence of adjacent compartments, especially axonal compartments. Therefore, I here used the base values of NaF, NaP and SK conductances, not the adjusted values for the somatic compartment. The conductances summarized in Table 1 are the reference values of our single-compartment model. In a later investigation, the conductances varied in the range between 50% and 150% of the reference values. We set the reversal potentials as E_{Na}=50 mV, E_K=−90 mV, E_{cat}=−30 mV, E_{Ca}=130 mV, and E_{leak}=−60 mV.

The gating variables obey the following kinetics:

$$\frac{dx}{dt} = \frac{x_\infty(z) - x}{\tau_x(z)},$$

where x represents a gating variable, and z is the membrane potential for a voltage-dependent variable or the internal calcium concentration for a calcium-dependent variable. x_∞ and τ_x are the activation or the inactivation function and the time constant, respectively, which for the voltage-dependent variable are given by the following equation:

$$x_\infty(V) = x_{\min} + \frac{(1 - x_{\min})}{1 + \exp[(\theta_x - V)/k_x]}$$
$$\tau_x(V) = \tau_x^0 + \frac{\tau_x^1 - \tau_x^0}{\exp[(\varphi_x - V)/\sigma_x^0] + \exp[(\varphi_x - V)/\sigma_x^1]}.$$

The time constant of the s gate of I_{NaP} were calculated from the equations:

$$\alpha_s(V) = \frac{A_s^\alpha V + B_s^\alpha}{1 - \exp[(V + B_s^\alpha/A_s^\alpha)/K_s^\alpha]},$$
$$\beta_s(V) = \frac{A_s^\beta V + B_s^\beta}{1 - \exp[(V + B_s^\beta/A_s^\beta)/K_s^\beta]},$$

Table 1 Conductances of the ionic channels (mS/cm^2)

g_{NaF}	50
g_{NaP}	0.1
g_{Kv2}	0.1
g_{Kv3}	10
g_{Kv4f}	2.0
g_{Kv4s}	1.0
g_{KCNQ}	0.2
g_{CaH}	0.3
g_{HCN}	0.1
g_{SK}	0.4
g_{leak}	0.068

and

$$\tau_s(V) = \frac{1}{\alpha_s(V) + \beta_s(V)}.$$

The detailed values of the parameters shown above are summarized in Table 2.

The intracellular calcium concentration $[Ca^{2+}]_i$ was determined from the following equation:

$$\frac{d[Ca^{2+}]_i}{dt} = -\frac{\gamma}{ZF} I_{CaH} - K_{Ca}([Ca^{2+}]_i - [Ca^{2+}]_{i0}),$$

where Z=2 is the valence of the calcium ion, F is the Faraday constant, $[Ca^{2+}]_{i0}$=0.01 μM is the baseline of $[Ca^{2+}]_i$, K_{Ca}=0.4 ms is the Ca^{2+} removal rate, and γ is the ratio of surface area to volume. We set γ to 30000 cm^{-1} so that the calcium transient, when an action potential was generated, would reach approximately 0.2–0.7 μM.

The kinetics of the SK current obeys the Hill equation:

$$m_\infty([Ca^{2+}]_i) = \frac{[Ca^{2+}]_i^{Hcoeff}}{(C_{50})^{Hcoeff} + [Ca^{2+}]_i^{Hcoeff}},$$

where H_{coeff}=4.6 is the Hill coefficient, and C_{50}=0.35 μM is the concentration producing a half effect. The time

Table 2 Parameters of the ionic channel kinetics

NaF	θ_m, k_m	−39, 5.0	Kv3	θ_m, k_m	−26, 7.8
	τ_m^0, τ_m^1	0.028, 0.028		τ_m^0, τ_m^1	0.1, 14
	θ_h, k_h	−48, -2.8		ϕ_m, σ_m^0, σ_m^1	−26, 13, -12
	τ_h^0, τ_h^1	0.25, 4.0		θ_h, k_h, h_{min}	−20, -10, 0.6
	ϕ_h, σ_h^0, σ_h^1	−43, 10, -5.0		τ_h^0, τ_h^1	7.0, 33
	θ_s, k_s, s_{min}	−40, -5.4, 0.15		ϕ_h, σ_h^0, σ_h^1	0, 10, -10
	τ_s^0, τ_s^1	10, 1000	Kv4f	θ_m, k_m	−49, 12.5
	ϕ_s, σ_s^0, σ_s^1	−40, 18.3, -10		τ_m^0, τ_m^1	0.25, 7.0
NaP	θ_m, k_m	−57.7, 5.7		ϕ_m, σ_m^0, σ_m^1	−49, 29, -29
	τ_m^0, τ_m^1	0.03, 0.146		θ_h, k_h	−83, -10
	ϕ_m, σ_m^0, σ_m^1	−42.6, 14.4, -14.4		τ_h^0, τ_h^1	7.0, 21
	θ_h, k_h, h_{min}	−57, -4, 0.154		ϕ_h, σ_h^0, σ_h^1	−83, 10, -10
	τ_h^0, τ_h^1	10, 17	Kv4s	θ_m, k_m	−49, 12.5
	ϕ_h, σ_h^0, σ_h^1	−34, 26, -31.9		τ_m^0, τ_m^1	0.25, 7.0
	θ_s, k_s	−10, -4.9		ϕ_m, σ_m^0, σ_m^1	−49, 29, -29
	A_s^α,B_s^α	−2.88e-6, -4.9e-5		θ_h, k_h	−83, -10
	K_s^α	4.63		τ_h^0, τ_h^1	50, 121
	A_s^β,B_s^β	6.94e-6, 4.47e-4		ϕ_h, σ_h^0, σ_h^1	−83, 10, -10
	K_s^β	−2.63	KCNQ	θ_m, k_m	−61, 19.5
Kv2	θ_m, k_m	−33.2, 9.1		τ_m^0, τ_m^1	6.7, 100
	τ_m^0, τ_m^1	0.1, 3.0		ϕ_m, σ_m^0, σ_m^1	−61, 35, -25
	ϕ_m, σ_m^0, σ_m^1	−33.2, 21.7, -13.9	CaH	θ_m, k_m	−20, 7.0
	θ_h, k_h, h_{min}	−20, -10, 0.2		τ_m^0, τ_m^1	0.2, 0.2
	τ_h^0, τ_h^1	3400, 3400	HCN	θ_m, k_m	−76.4, -3.3
				τ_m^0, τ_m^1	0, 3625
				ϕ_m,	−76.4,
				σ_m^0, σ_m^1	6.56, -7.48

constant τ_m is $\tau^1 - \frac{(\tau^1-\tau^0)[Ca^{2+}]_i}{[Ca^{2+}]_{sat}}$ if $[Ca^{2+}]_i < [Ca^{2+}]_{sat} =$ 5.0 μM, where τ^0=4.0 ms and τ^1=76 ms. The other parameters are summarized in Table 2.

2.2 Synaptic model

GPe neurons have GABAergic axonal collaterals. A $GABA_A$ synaptic current was described by the following formula:

$$I_{syn} = g_{syn} s (E_{syn} - V),$$

where g_{syn} and E_{syn} are the maximal conductance and reversal potential, respectively. The variable s represents the open probability and obeys the following first-order kinetics (Destexhe et al. 1998):

$$\frac{ds}{dt} = \alpha R(1-s) - \beta s,$$

where α and β are the activation and deactivation rates, respectively. Variable R is 1 when the presynaptic membrane potential exceeds 0 mV and is 0 otherwise. α is 5.0 ms^{-1} and β is 0.18 ms^{-1}. E_{syn} was set to −75 mV. We assumed that the conduction delay from a presynaptic neuron to a postsynaptic neuron was 1 ms.

2.3 Phase response analysis

We considered that GPe neurons show periodical firing activity. The dynamic system exhibiting periodic activity on a stable limit cycle can be represented by a single-phase variable (Ermentrout and Kopell 1984; Kuramoto 1984). Furthermore, if the interaction between such oscillatory units is sufficiently weak, the dynamics of coupled oscillatory units can be reduced to the dynamics of coupled phase oscillators. By investigating the stable phase differences between coupled phase oscillators, we can understand how a larger network of oscillators behaves. If the stable phase difference between phase oscillators is 0, the larger network is expected to exhibit global synchrony. We applied this method to coupled GPe neurons to understand which parameters exert a significant influence on network activity.

The dynamic equation of a neuron showing periodic activity can be reduced to the following equation of phase variable ϕ:

$$\frac{d\phi}{dt} = \frac{2\pi}{T} + Z(t) I_{syn}(t),$$

where T is the period of firing activity, and $Z(t)$ is the so-called phase response function representing the amount of phase advance, with a small perturbation at time t. The synaptic input to the periodically firing neuron, $I_{syn}(t)$, is also calculated as a periodic function, based on the assumption that the presynaptic neuron fires at the same firing rate. In general, $Z(t)$ takes positive or negative values depending on t. If $Z(t)$ is positive at t, a small depolarizing perturbation at t advances the next action potential. $Z(t)$ was numerically obtained by solving the adjoint equation numerically (Ermentrout 1996; Hoppensteadt and Izhikevich 1997; Nomura et al. 2003; Takekawa et al. 2007).

Considering that 2 GPe neurons are mutually connected by synapses, we obtained the following 2 equations:

$$\frac{d\phi_1}{dt} = \frac{2\pi}{T} + g_{syn}\,\Gamma(\phi_1 - \phi_2)$$
$$\frac{d\phi_2}{dt} = \frac{2\pi}{T} + g_{syn}\,\Gamma(\phi_2 - \phi_1),$$

where ϕ_1 and ϕ_2 are the states of the coupled neurons, and the interaction function Γ takes the following form:

$$\Gamma(\phi) = \frac{1}{T} \int_0^T Z(\tau) s\left(\tau - \frac{\phi T}{2\pi}\right)(E_{syn} - V(\tau))\,d\tau.$$

Γ is a periodic function depending on only the phase difference, $\Delta\phi = \phi_1 - \phi_2$. Therefore, the dynamic equation of the phase difference can be obtained as follows:

$$\frac{d\,\Delta\phi}{dt} = \Gamma_{odd}(\Delta\phi) \equiv \Gamma(\Delta\phi) - \Gamma(-\Delta\phi).$$

Stable solutions of this equation give stable firing patterns of the coupled neurons. If $\Delta\phi$=0 is a stable solution, the neurons synchronize in the steady state. The conditions of stable fixed points are as follows:

$$\Gamma_{odd} = 0 \quad \text{and} \quad \frac{d\,\Gamma_{odd}}{d\,\Delta\phi} < 0.$$

In a later analysis, we observed how stable solutions satisfying these conditions depended on parameters such as ionic conductances.

To validate the results obtained from the phase response analysis, we conducted numerical simulations of two-coupled neurons and a network of 64 GPe model neurons. In the simulation of the two-coupled neurons, we confirmed the stable phase difference of the 2 neurons by changing the synaptic conductance to see the range in which the weak-coupling assumption is applicable. The applied current (I_{app}) to both neurons was 3.0 μA/cm^2. Initially, an asynchronous state was generated for 5000 ms by setting the initial membrane potentials and synaptic conductance to random and 0, respectively. Then, synaptic connections with g_{syn} were introduced. After a certain transient time, the stable phase difference between the pair of neurons was obtained. We performed this procedure for 2 sets of conductances. In one case, all the conductances were set to the reference values, which yield the monostable in-phase state. In the other set, g_{NaP} and g_{Kv3} were decreased

from the reference values by 20%, whereas g_{KCNQ} and g_{SK} were increased by 20%. The model with this set of conductances showed bistability of the in-phase and antiphase states. The network model consisted of 64 GPe neurons that had all-to-all synaptic connections. In the network simulation, the synaptic conductance was set to 0.02 mS/cm^2—that is, estimated at about 0.56 nS, given that the soma is a sphere with a diameter of 15 μm (Cooper and Stanford 2000). The applied current varied by neuron and was defined as $I_{app}=I_{app,0}+\sigma_I\eta$, where $I_{app,0}$ and σ_I are the mean and standard deviation, respectively. η obeyed the normalized Gaussian distribution $N(0, 1)$. We set $I_{app,0}$ to 3.5 μA/cm^2, whereas σ_I was changed from 0 to 0.3 μA/cm^2. The conductances that would have effects on PRC were set as $g_{NaP}=g_{NaP,0}(1-q)$, $g_{Kv3}=g_{Kv3,0}(1-q)$, $g_{KCNQ}=g_{KCNQ,0}(1+q)$, and $g_{SK}=g_{SK,0}(1+q)$, where $g_{X,0}$ is the reference value of the conductance g_X. When $q=0$, those conductances assume the reference values. In case of $q=0.2$, g_{NaP} and g_{Kv3} were decreased, and g_{KCNQ} and g_{SK} were increased, which made both antiphase and in-phase states stable. In contrast, the conductances for $q=-0.2$ made monostable in-phase synchrony more robust. The network simulation was conducted for the 3 cases of conductance settings. To characterize the degree of synchrony in the network, we calculated the coherence measure for a pair of neurons—i and j (Wang and Buzsáki 1996):

$$\kappa_{ij}=\frac{\sum_t x_i(t)x_j(t)}{\sqrt{\sum_t x_i(t)\sum_t x_j(t)}},$$

where $x_i(t)$ denotes a binary variable that represents whether neuron i evokes a spike (1) or not (0) between t and $t+\Delta t$. We defined the network synchrony as the measure averaged over all possible pairs in the network, $\kappa=\langle\kappa_{ij}\rangle_{ij}$. The time bin Δt was determined by the value when κ, for various bin sizes, was at its maximum.

The numerical analysis of PRC and the simulation were conducted by C/C++ programming, and the integration was performed by the 5th-order and the 4th-order Runge–Kutta method, respectively. The time step of the simulation was 0.01 ms. Our modified version of a single-compartmental GPe neuron is uploaded in ModelDB.

3 Results

Figure 1(a) shows the simulations of step current injection to the model GPe neuron. Before current injection, the model neuron showed autonomous activity at 8 spikes/s. Following hyperpolarizing current injection, the membrane potential was gradually depolarized after rapid hyperpolarization was observed. This gradual depolarization is due to the contribution of the HCN current that generates a depolarizing current in response to membrane potential hyperpolarization. Figure 1(b) illustrates the profiles of ionic currents during periodic firing. The current through the NaF channels exhibited a very sharp change, whereas the other currents showed similar time courses to the change in membrane potential. The I-F curve of the model neuron is shown in Figure 1(c). As the intensity of the applied current increased, the firing rate of the model neuron monotonically increased and reached more than 100 spikes/s (113 spikes/s) when I_{app} was 10 μA/cm^2. This high frequency spiking is generated by the Kv3 potassium channel (Baranauskas et al. 1999).

We applied phase response analysis to our model GPe neuron (Ermentrout and Kopell 1984; Kuramoto 1984). The method requires the assumption that a neuron exhibits periodic firing activity. The firing period was adjusted by changing the magnitude of I_{app}. Figure 2 illustrates a typical example of the analysis when the firing period was set to 20 ms by applying a steady current of 2.9 μA/cm^2. V is the waveform of the periodic firing. For convenience, we defined the starting point of repolarization as the onset of the period. Z is the phase response curve representing the degree of phase advance or delay following an infinitesimal depolarizing perturbation of the membrane potential. If the perturbation at t contributes to an advance in the next action potential, $Z(t)$ is positive. As shown in the figure, Z for this set of parameters had a negative component at the repolarization phase after the action potential, whereas Z was positive at the other phase. Here, we consider the case where a pair of identical neurons has mutual synaptic connections. The time course of the open gate probability of a synapse, s, is activated when the presynaptic membrane potential exceeds 0 mV and neurotransmitters are released from the presynaptic terminals. It should be noted that we introduced a synaptic delay of 1 ms in this case. The interaction function, Γ, is an integral of the product of the phase response, Z, and a synaptic input from the other neuron, I_{syn}—which represents an actual contribution of a synaptic input to the phase advance or delay during the period. Γ governs the dynamic changes in the phase variables representing the states of the mutually coupled model GPe neurons. As Γ depends only on the difference between the phases of the 2 neurons, we finally obtain the dynamic equation of the phase difference (see Section 2 for details). The odd component of Γ, Γ_{odd}, plays an important role in determining the stable states of this dynamics. The fixed points satisfying $\Gamma_{odd}=0$ and $d\Gamma_{odd}/d\Delta\phi<0$ are stable phase differences; that is, the coupled neurons periodically fire by maintaining a time difference corresponding to the phase difference. In Figure 2, the fixed points are indicated by closed circles. The result indicates that the neurons exhibit an in-phase synchronization.

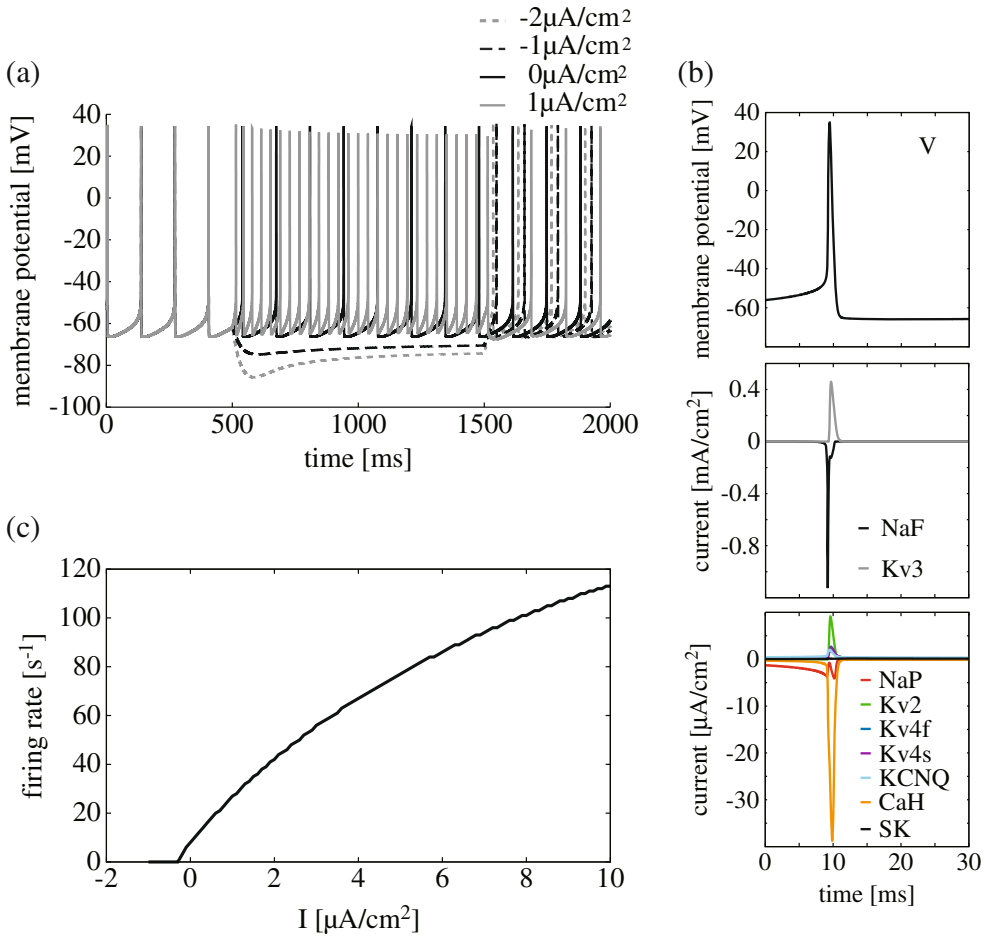

Fig. 1 Responses to current injections. (**a**) Responses to depolarizing and hyperpolarizing step currents. The applied current, I_{app}, was set to −2.0, −1.0, 0, and 1.0 μA/cm^2 from 500 ms to 1500 ms and to 0 μA/cm^2 before and after this duration. The model neuron showed autonomous activity at 8 spikes/s when no external current was applied. During the hyperpolarizing current injection, voltage sags were observed. After release from this current injection, rebound firings at a higher firing frequency than the autonomous firing frequency were evoked. (**b**) Shapes of membrane potential and ionic currents during action potential generation. Top: membrane potential. Middle: fast transient sodium current (I_{NaF}) and fast delayed rectifier current (I_{Kv3}) that are responsible for action potential generation. Bottom: the other currents. (**c**) IF curve of the model neuron. The firing frequency gradually increased with increased intensity of I_{app}. When I_{app}=10 μA/cm^2, the frequency reached more than 100 spikes/s

We then studied the effect of a change in ionic conductance on the phase response of the GPe neuron. We obtained the PRC by changing one of the ionic conductances (but not g_{NaF}) from 50% to 150% of the respective reference value shown in Table 1. I_{app} was set to 2.9 μA/cm^2 so that the period of neuronal activity was maintained at 20 ms for the set of reference conductances. Figures 3(a)–(g) show the phase responses obtained when the conductance of the target ionic current was set to $g^{ref}\times0.5$, g^{ref}, and $g^{ref}\times1.5$, and the other conductances were set to the reference values. The changes in g_{Kv2} (b), g_{Kv4f} (d), g_{Kv4s} (not shown), and g_{HCN} (not shown) had only a subtle effect on the phase response. On the other hand, changes in g_{NaP} (a), g_{Kv3} (c), g_{KCNQ} (e), g_{CaH} (f), and g_{SK} (g) altered the shape of the phase response. The conductances of potassium currents—g_{Kv3}, g_{KCNQ}, and g_{SK}—primarily affected the PRC in the timing after an action potential (small ϕ<0.5). g_{NaP} exerted its effect on the PRC in the timing before an action potential (large ϕ>0.5), as well as slightly for small ϕ. Small g_{CaH} largely altered the PRC, whereas an increase in g_{CaH} only scaled down the PRC without changing its shape. Since the applied current was maintained at the same magnitude, changes in the conductances may have altered the firing period. Figure 3(h) shows the dependence of the firing period on the conductance changes. Increases in g_{NaP} and g_{Kv3} decreased the firing period (increased the firing rate), whereas increases in g_{KCNQ}, g_{CaH}, and g_{SK} increased the firing period. The increase in the firing period by a larger g_{CaH} is due to the activation of the SK current by the increased calcium influx.

Using the previous results of Z, we computed the interaction function and Γ_{odd}. As the effects of g_{Kv2}, g_{Kv4f}, g_{Kv4s}, and g_{HCN} on Z and the firing period were negligible

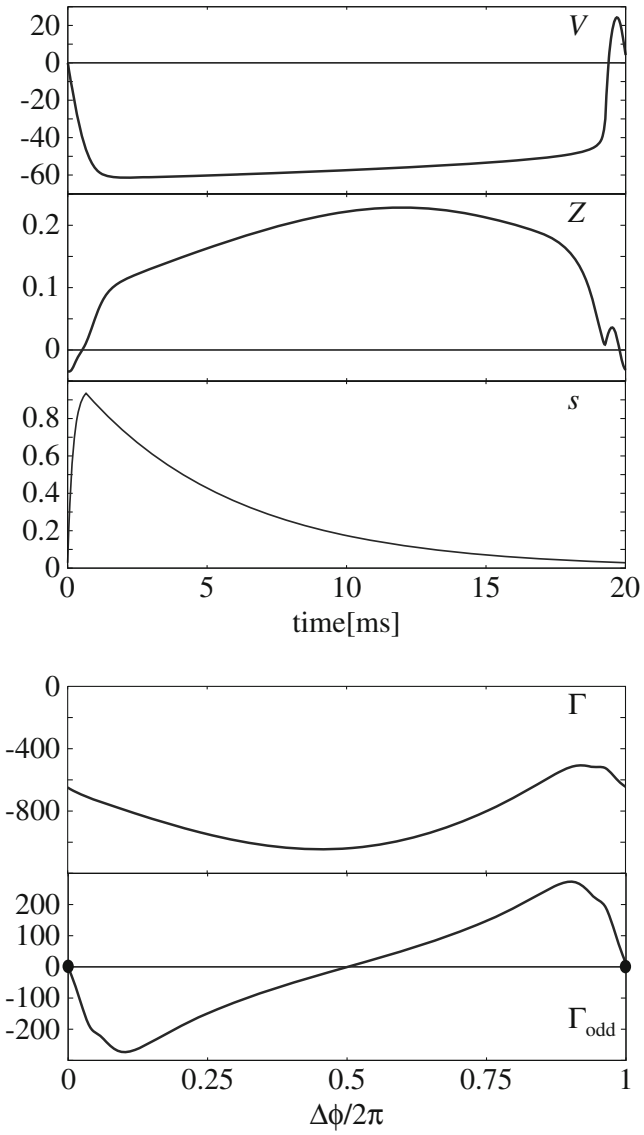

Fig. 2 An example of a phase response curve. *V* represents a periodic orbit of a membrane potential, *Z* is the phase response curve of the orbit, and *s* is the rate variable of a synaptic current. This profile of *s* was obtained from *V* with a synaptic delay of 1 ms. The interaction function, Γ, was calculated from *Z*, *V*, and *s* determined by the presynaptic neuron (see Section 2) and depends on the phase difference between the presynaptic and the postsynaptic neurons. Γ_{odd} is the odd part of Γ. The open circles indicate the phase differences satisfying conditions $\Gamma_{odd}=0$ and $d\Gamma_{odd}/d\Delta\phi<0$. These are the stable phase differences that coupled neurons show after long time. All the conductances were set to the reference values in Table 1 and I_{app}= 2.9 μA/cm^2

under the assumed conditions, Γ_{odd} for these conductances also showed no remarkable differences between different values of the conductances (data not shown). In Fig. 4, Γ_{odd} and stable phase differences are indicated for g_{NaP}, g_{Kv3}, g_{KCNQ}, and g_{SK}. As shown in Fig. 4(a1) and (b1), for g_{NaP} and g_{Kv3}, an increase in the conductance resulted in a steeper slope of Γ_{odd} at the antiphase difference $\Delta\phi=\pi$. In particular, when g_{Kv3}=5 mS/cm^2, the slope at $\Delta\phi=\pi$ became negative. An increase in g_{KCNQ} and g_{SK} yielded a milder slope at $\Delta\phi=\pi$ (c1 and d1); however, the slopes remained positive. Figure 4(a2), (b2), (c2), and (d2) illustrate stable phase differences for the varied conductances. All the displayed Γ_{odd} values had a stable solution at $\Delta\phi=0$, which means in-phase synchronization was stable for a pair of model neurons. As long as the conductances were changed within the specified range, the changes (except for the case of g_{Kv3}) had no influence on the stable states, namely, in-phase synchronization is a unique stable state. As for the change in g_{Kv3}, a stable state at the antiphase $\Delta\phi=\pi$ emerged when g_{Kv3}=5 mS/cm^2 (Fig. 4 (b2)), which suggests that antiphase synchronization becomes stable as g_{Kv3} becomes smaller.

To examine how the stability of the phase difference depends on the conductances and the firing period, we analyzed the cases of 16.7 ms and 25 ms, which correspond to 60 spikes/s and 40 spikes/s, respectively. The applied current was adjusted to 3.9 μA/cm^2 for T=16.7 ms and 2.1 μA/cm^2 for T=25 ms. We focused on g_{NaP}, g_{Kv3}, g_{KCNQ}, and g_{SK}, because the other conductances had no effect on the steady-state solutions (not shown). Figure 5 shows the dependence of stable phase differences on the conductance changes in case of the shorter firing period (T=~16.7 ms) and the longer one (T=~25 ms). When the input current was decreased (T=~25 ms), a small g_{NaP} (<0.064 mS/cm^2) stabilized not only the in-phase state but also the antiphase difference. In comparison with the case of T=~20 ms (Fig. 4(b2)), the boundary of Kv3 conductance between bistable and monostable states increased from 5.0 to 7.4 (Fig. 5(b1)). As for g_{KCNQ}, the transition point of the stable antiphase difference emerged at 0.284 in the case of T=~25 ms (Fig. 5(c2)). The change in g_{SK} affected stable solutions only when the firing period was decreased to about T=~16.7 ms (Fig.5(d1)). In all cases, the in-phase synchronization was stable for the entire range of conductances. However, the stability of the antiphase state depended on both the firing period and the ionic conductances. In the case of g_{NaP}, the antiphase difference became stable when g_{NaP} was reduced, for the longer firing period (T=~25 ms). Reducing g_{NaP} increased the firing period (Fig.3(h)). This indicates that the long period could make the antiphase difference stable. As for g_{KCNQ}, the stable antiphase difference emerged for the larger conductance and the longer period. It should also be noted that an enhanced g_{KCNQ} increases the period. Similar to the case of g_{NaP}, the prolonged firing period by an enhanced g_{KCNQ} stabilized the antiphase difference. Thus, the stability of the antiphase difference may be related to the length of the firing period brought by the change in these 2 currents, rather than the conductance change per se.

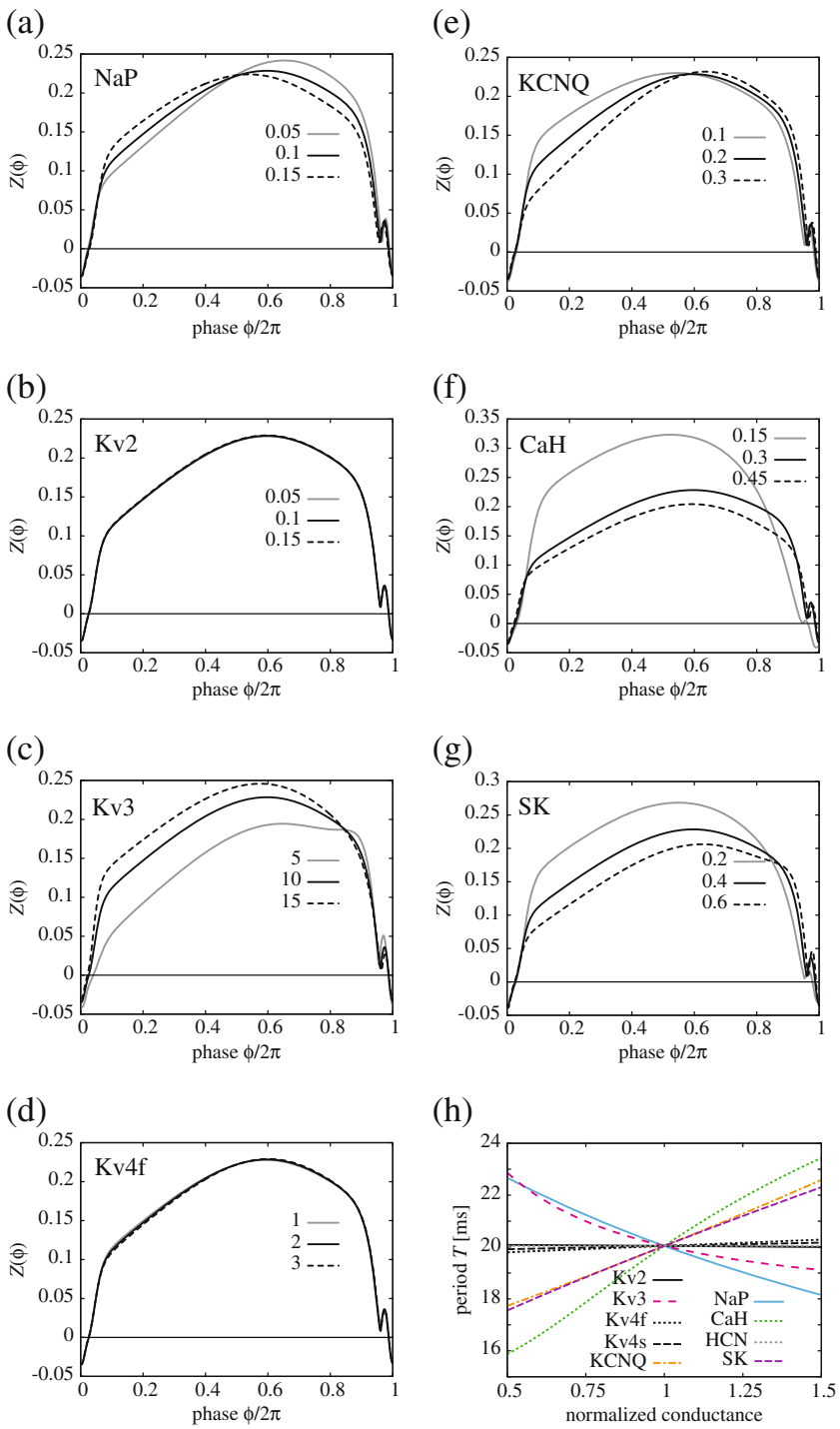

Fig. 3 Dependence of phase response curves (PRCs) on conductance changes. (**a**) g_{NaP}, (**b**) g_{Kv2}, (**c**) g_{Kv3}, (**d**) g_{Kv4f}, (**e**) g_{KCNQ}, (**f**) g_{CaH}, and (**g**) g_{SK}. The PRCs were calculated in the condition where one of the conductances was varied and the others were set to the reference values in Table 1. In (**a**)–(**g**), the results for 50%, 100%, and 150% of the reference values are indicated. The horizontal axis represents phase $\phi/2\Pi$, corresponding to the time normalized by the firing period. I_{app} was set to 2.9 μA/cm^2. (h) Change in the firing period when a conductance was varied

On the other hand, Kv3 and SK currents presumably contributed to the stability in a different manner. As shown above, we could confirm that the antiphase difference was stable when the phase response at the early phase (small ϕ) was small (Fig. 3). In order to clarify the contribution of the change in these conductances to the reduced phase response at the early phase, it is necessary to remove the effects of the length of the firing period. For this purpose, we compared 2 sets of parameters that yielded the same firing period but different results of the antiphase difference stability. In Figure 6(a), the waveforms of membrane potential, phase response, and SK conductance are shown for the 2 sets. The parameter set of g_{SK}=0.536 mS/cm^2 and I_{app}=3.9 μA/cm^2 generated a stable antiphase difference, whereas the antiphase difference was unstable for the other set—g_{SK}=0.232 mS/cm^2 and I_{app}=2.9 μA/cm^2. Although the waveforms of the membrane potential are the same (top), the phase response curves are quite different from

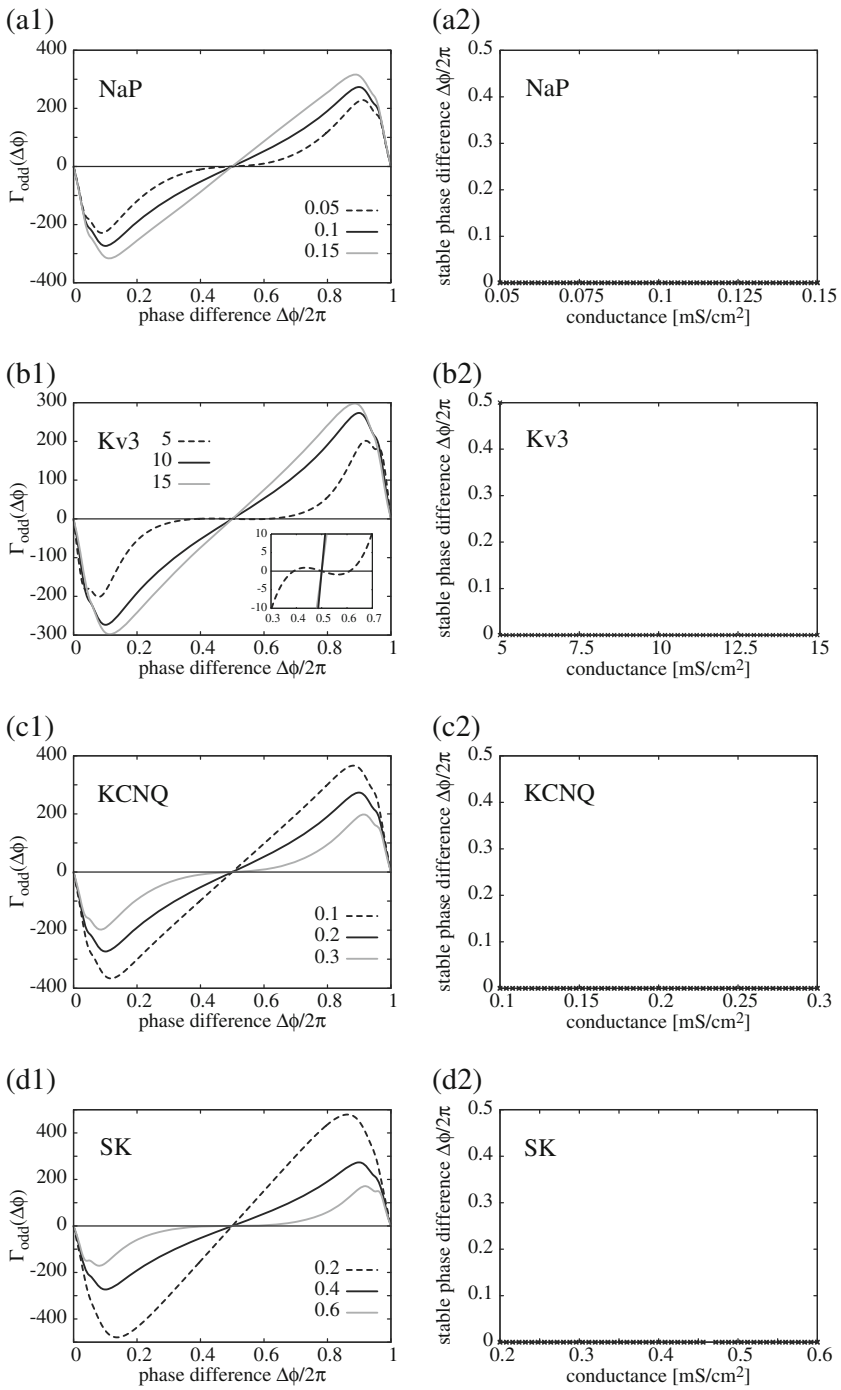

Fig. 4 Γ_{odd} and stable phase differences. On the basis of the results shown in Fig. 3, the odd part of the interaction function, Γ_{odd}, was obtained. (a1)–(d1) The dependence of Γ_{odd} on a change (50%, 100%, and 150%) in the reference value of the target conductance. (a2)–(d2) The dependence of the stable phase differences on the conductance change. A cross (x) indicates the existence of a stable phase difference at a given value of the conductance. The existence of two stable phase differences at a given value of the target conductance means that those phase differences are bistable

each other (middle). In particular, the phase response at early phase (ϕ<0.5) is much smaller for the case of larger g_{SK}. This can be attributed to an increase in the SK conductance at the early phase (bottom). We next examined the impact of such an asymmetrical change in PRC on the stability of antiphase synchrony. Fig. 6(b) illustrates how 2 coupled neurons behave when the SK conductance changes. We should note that g_{SK}=0.536 produces stable antiphase synchrony, whereas g_{SK}=0.496 destabilizes the antiphase synchrony, and that the interaction function $\Gamma(\phi)$, which represents a phase advance caused by synaptic input, became entirely negative because the neuron received inhibitory synaptic inputs. We now consider the case that 2 neurons, neurons 1 and 2, show antiphase synchrony for g_{SK}=0.536, and then g_{SK} changes from 0.536 to 0.496. Because of the change in conductance, $\Gamma(\phi)$ decreased, particularly at the early phase. This decrease in $\Gamma(\phi)$ further delays the subsequent spike if the synaptic input was applied at the early phase. Therefore, a synaptic input from neuron 2 (the left cyan arrow) delayed the subsequent spike

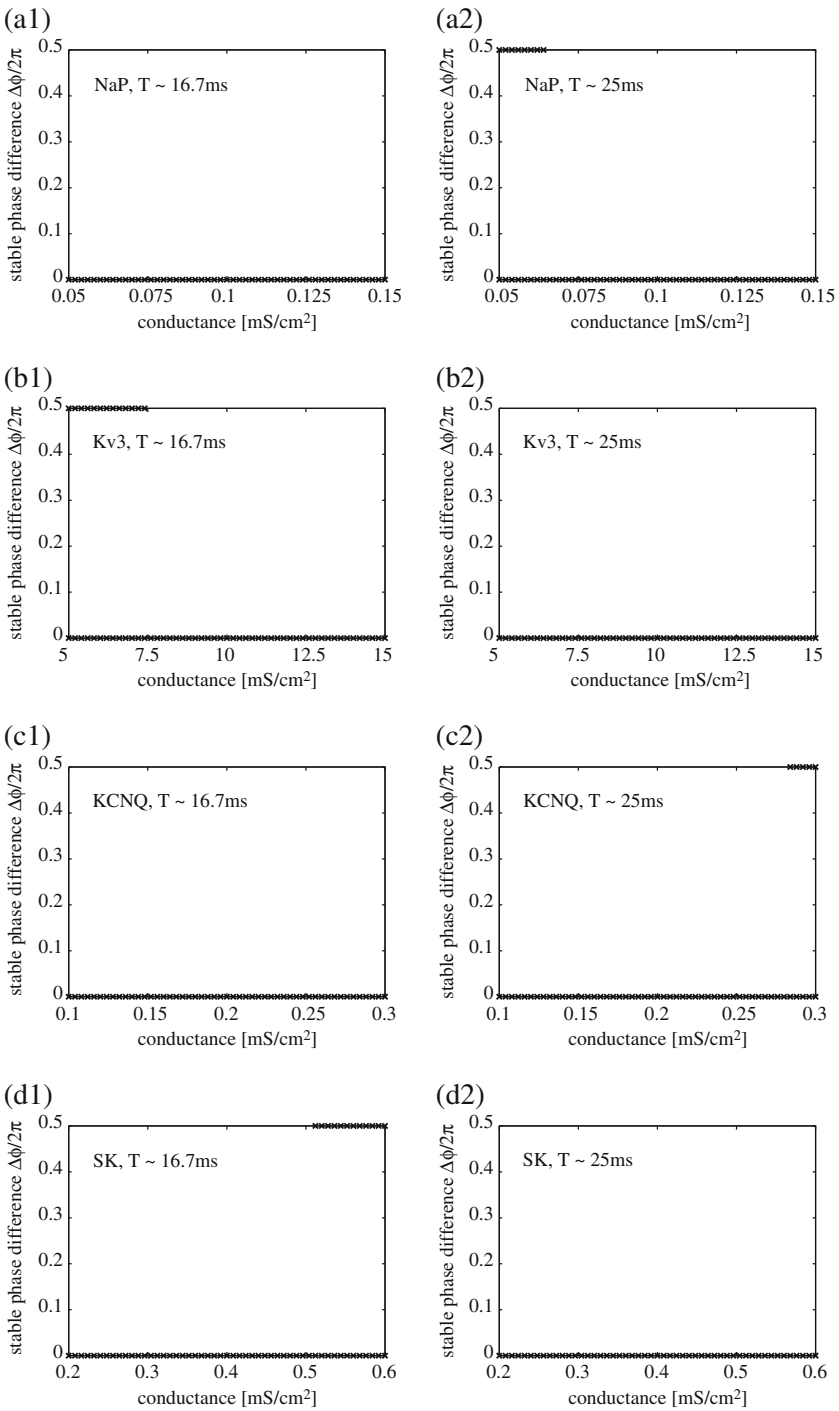

Fig. 5 Stable phase differences in different firing periods. (a1)–(a4) I_{app} was set to 3.9 μA/cm^2 so that the firing period was about 16.7 ms (~60 spikes/s). (b1)–(b4) I_{app} was set to 2.1 μA/cm^2 so that the firing period was about 25 ms (~40 spikes/s)

of neuron 1. In turn, a synaptic input from neuron 1 (the left black arrow) was given to neuron 2. However, because the timing is at ϕ>0.5, where a decrease in $\Gamma(\phi)$ was relatively small, the spike timing of neuron 2 is not influenced. Thus, the spike timing of neuron 1 is delayed by inputs at the early phase, whereas neuron 2 maintains firing pace while receiving inputs at the late phase. This is because the asymmetrical modification of $\Gamma(\phi)$ destabilizes the anti-phase synchrony.

The combined effect of the conductance changes on the steady states of the coupled neurons was investigated. We studied how pairs of g_{Kv3}, g_{NaP}, g_{KCNQ}, and g_{SK} influence the stability of the antiphase difference. In Figure 7, each square indicates that the antiphase difference was stable for a pair of conductance values. As shown in the figures (a–c), the stability changed depending on the combination of both conductances. For example, when g_{NaP} was set to the reference value of g_{NaP}=0.1, the antiphase difference was

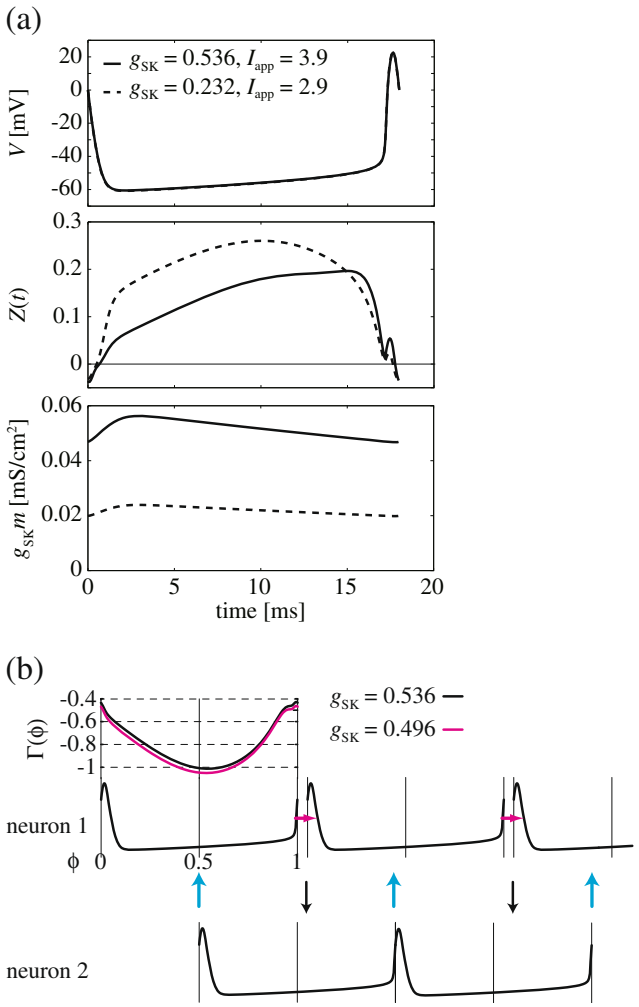

Fig. 6 An asymmetrically altered interaction function $\Gamma(\phi)$ destabilizes antiphase synchrony. (**a**) Profiles of membrane potential (*top*), phase response (*middle*) and SK conductance (*bottom*) during periodic firing for different parameter sets, but with the same period. The solid lines are the profiles for the case of g_{SK}=0.536 and I_{app}=3.9 that made both $\Delta\phi$=0 and Π stable. The broken lines are the ones for g_{SK}=0.232 and I_{app}=2.9 for which only the in-phase state is stable. (**b**) Phase response or interaction function change at early phase determines the stability of antiphase synchrony. The interaction functions for different SK conductance g_{SK}=0.536 and 0.496 but the same applied current I_{app}=3.9 are shown by black and magenta lines, respectively. It is depicted how coupled neurons, neuron 1 and 2, showing antiphase synchrony with g_{SK}=0.536 changed their activity if g_{SK} is changed to 0.496 for which only the in-phase synchrony is stable. Black and cyan arrows indicate timings of synatic inputs from neuron 1 and 2, respectively. Magenta arrows show a relative phase shift produced by a change in g_{SK} and timing of a synaptic input

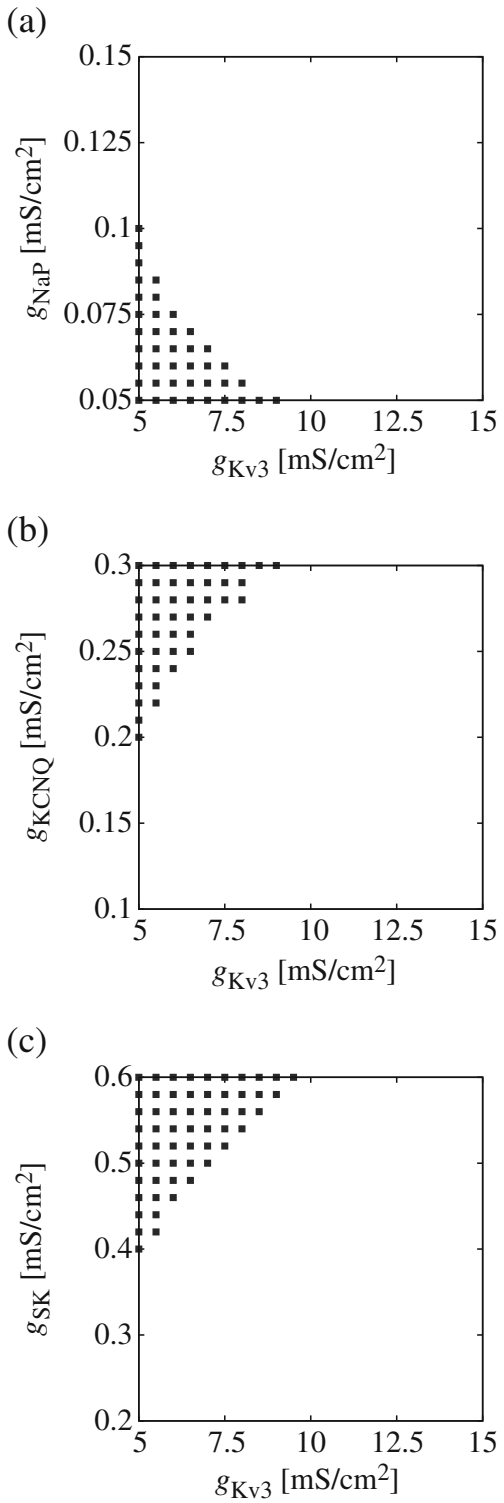

Fig. 7 The stability of the antiphase difference depended on a combined change in two conductances. The crosses (x) represent stable antiphase differences ($\Delta\phi=\Pi$) when two conductances were independently varied. The in-phase difference ($\Delta\phi$=0) was always stable. Phase diagrams for (**a**) g_{Kv3} and g_{NaP}, (**b**) g_{Kv3} and g_{LCNQ}, and (**c**) g_{Kv3} and g_{SK} are shown

stable only at g_{Kv3}=5 (Fig. 6(a)), as seen previously (Fig. 4 (b2)). As g_{NaP} was decreased, even larger g_{Kv3} yielded a stable antiphase difference. This occurred only when g_{NaP} decreased, which is consistent with the result seen when only the conductance was changed (Fig. 5(a2)). For the other combination, a similar tendency was confirmed: the simultaneous change enabled even small changes in each

conductance to stabilize the antiphase difference, and an emerging trend of stable antiphase difference was consistent with the previous results.

Finally, we validated the above phase response analysis by using numerical simulation of two-coupled neurons and a GPe network model. The phase response analysis assumes an infinitesimal perturbation—in other words, an infinitesimally small interaction between neurons. We therefore first confirmed whether the magnitude of synaptic interaction altered the stable states that were obtained under the weak-coupling condition. A pair of neurons using the reference values of conductances showed the monostable in-phase synchrony, whereas the pair of neurons with decreased g_{NaP} and g_{Kv3} and increased g_{KCNQ} and g_{SK} had stable antiphase states as well as stable in-phase states. Numerical simulations for the 2 cases of two-coupled neurons were conducted with varied synaptic conductances. Figure 8(a) indicates stable phase differences for different magnitudes of synaptic conductance. The coupled neurons using reference values for conductances showed in-phase synchrony for the synaptic conductance up to 0.3 mS/cm^2 (solid line). For the bistable case, the antiphase state remained stable as the synaptic conductance increased up to 0.1 mS/cm^2 (broken line). In both cases, the coupled neurons with a large synaptic conductance strongly inhibit each other and no longer remain in a 1:1 phase-locked state. We next conducted simulations of a network model, in which 64 GPe neurons have all-to-all synaptic connections. In this network simulation, the firing period of a neuron differed because the applied current to a neuron was determined randomly (see Section 2). Figure 8(b1) and (b2) are raster displays for σ_I=0 and 0.3, respectively. The raster displays show the spike activities for different conductance settings that are represented by the parameter q, a factor shifting the balance between intrinsic membrane conductances shown to impact the PRC shape (also see

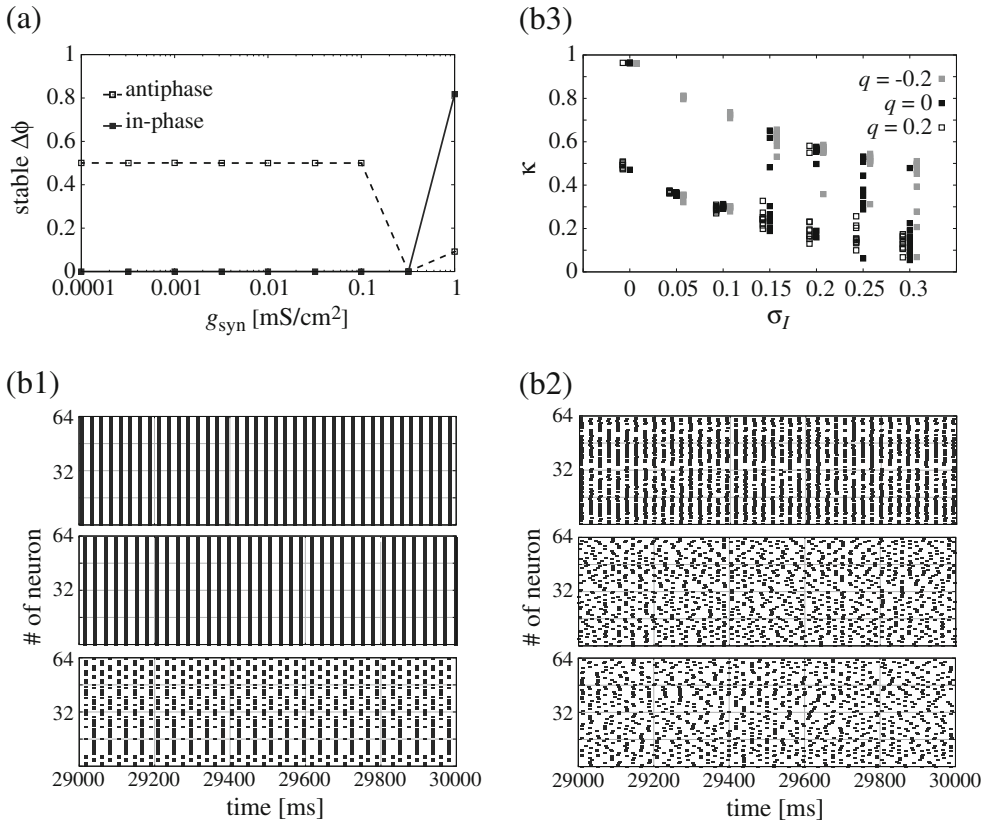

Fig. 8 Numerical simulations of two-coupled neurons and a mutually connected GPe network. (**a**) Dependence of stable states on the strength of synaptic conductance. Whether an increase in the synaptic conductance between two neurons changes the stable states was investigated for the conductance configurations of the unique in-phase synchrony (*in-phase*, *solid line*) and of the antiphase synchrony (*antiphase*, *broken line*) in the theoretical analysis with PRC. (**b**) The degree of synchrony in a network of 64 GPe neurons. We introduced the parameter q that represents a rate of change of the condutances shown to impact the PRC shape (see Section 2). (b1) spike raster displays for an identical applied current (σ_I=0) but different membrane properties: conductances with q=−0.2 to make the in-phase synchrony robust (top), reference conductances with q=0 (middle) and conductances with q=0.2 to stabilize the antiphase synchrony (bottom). (b2) similar to (b1), but in the case that the applied currents were different neuron by neuron (σ_I=0.3). (b3) the degree of network synchrony, κ, that was defined as the coherence measure averaged over all possible pairs of neurons. The results of 10 trials for each parameter set of q and σ_I are illustrated

Section 2). In Fig. 8(b1), the network with q=−0.2 and 0 exhibited global synchronization (top and middle). On the other hand, the neurons in the network with q=0.2 were separated into 2 clusters, showing antiphase synchrony (bottom). Figure 8(b2) is similar to 8(b1), but the firing rates were different in each neuron. For q=−0.2, the network almost exhibited global synchronization, but some neurons, which presumably received weaker applied current, failed to fire or fired at firing rates lower than the firing rates without synaptic interaction. When q=0 and 0.2, the network exhibited almost asynchronous spiking activity. To quantitatively characterize the degree of network synchrony, we calculated the coherence measure averaged over all possible neuron pairs in the network (Wang and Buzsáki 1996). Figure 8(b3) summarizes the averaged coherence measures of 10 trials, depending on the standard deviation of the applied current σ_I. As shown in the figure, κ decreased as σ_I increased. The decaying upper bound starting from κ~1 at σ_I=0 and the decaying lower bound from κ~0.5 at σ_I=0 corresponded to the in-phase and antiphase synchrony, respectively. The network of neurons showing bistability, in terms of synchrony (q=0.2), showed asynchronous activity (open squares). On the other hand, the network of neurons having robust in-phase synchrony (q=−0.2) tended to synchronize globally (gray squares). In the case of q=0, the degree of synchrony was statistically an intermediate value between the cases of q= 0.2 and −0.2. Thus, the network simulation indicated that the model with the reference conductances yielded an asynchronous state if the variability of firing rates was increased. What we address here is the tendency that cellular plasticity, particularly changes in the conductance responsible for the PRC shape, could trigger a transition of network activity, rather than the result that theoretical analysis revealed global synchrony was stable under the normal condition where the neurons had the reference values of the conductances.

4 Discussion

The activity of GPe neurons exerts a significant impact on STN neurons, especially in relation to the rebound burst activity frequently observed in STN neurons under a pathological condition. Since synchronous activity in GPe neurons presumably induces such pathological burst activity (Bevan et al. 2000; Hallworth and Bevan 2005), we studied the possible mechanisms inducing synchrony in GPe neurons by focusing on membrane property modulation. To investigate how changes in the ionic channels on the membrane contribute to synchrony in GPe neurons, we applied phase response analysis to the model GPe neuron by changing the conductances of the ionic channels. By this method, we studied the stability of the phase difference between coupled GPe neurons with a given set of conductances. If zero phase difference ($\Delta\phi$=0) is the unique steady state in the analysis, the results suggest that the network of GPe neurons exhibited global synchronization.

We confirmed that some ionic channels had little impact on the steady-state activity of the coupled GPe neurons, whereas others had a certain impact. The conductance change in Kv2, Kv4f, Kv4s, and HCN currents did not alter the stable phase difference. Since HCN currents are activated only when the membrane potential is hyperpolarized, these ionic channels exerted less influence under the condition where the neuron displayed periodic firing activity at the spike threshold level. In the periodic firing mode with singlet spikes, NaP, Kv3, KCNQ, CaH, and SK currents had a considerable impact on PRC, and consequently Γ_{odd}. However, the CaH current did not stabilize the antiphase difference, whereas changes in the magnitudes of NaP, Kv3, KCNQ, and SK currents yielded a stable antiphase difference, depending on the firing period. As illustrated in Fig. 3(h), an increase in g_{CaH} did not increase but decreased the firing rate. This is because an increased calcium influx activated the calcium-dependent potassium channels, SK channels, and caused a hyperpolarizing effect, like that of the potassium channels. Although the change in g_{CaH} showed a similar result to a change in g_{SK}, its indirect effect through the SK channel was presumably weak at the early phase.

The shape of the PRC defines the function of Γ_{odd}, and consequently, the stable states. As seen in Fig. 3, reduction of the phase response at early phase (small ϕ) played an important role for the stable states and depended on both the ionic conductances (NaP, Kv3, KCNQ, and SK) and the firing period. We could separate this dependency into 2 types: changes in NaP and KCNQ currents caused extension of the firing period and a shift in the peak of the PRC (Fig. 3(a) and (e)), whereas decrease in the Kv3 current weakens action potential repolarization, and consequently, the membrane potential was slightly depolarized immediately after an action potential (not shown). This caused enhancement of the slow potassium currents from I_{KCNQ} and I_{SK}. On the other hand, an increase in the SK current directly increased the slow potassium current. The slow potassium current was likely to prevent phase advance, especially at the early phase. Thus, the mechanism responsible for the level of the slow potassium current is likely to directly or indirectly control the stable state in the GPe network (Fig. 6).

The theoretical analysis of the PRC assumes a phase response to infinitesimal perturbation. Therefore, a biologically plausible perturbation like a synaptic input would alter the shape of the PRC because of the nonlinearity of membrane properties, and consequently lead to a different

steady-state activity. To confirm this, we demonstrated numerical simulations of the two-coupled neurons and the network model. In the simulation of the coupled neurons, although the membrane potential profile during periodic firing was distorted in the case of strong synaptic inputs, the stability of both in-phase and antiphase synchrony was not disturbed, even if the synaptic conductance was increased up to 0.1 mS/cm^2 (~2.8 nS). In the network simulation, an increase in the variability of the applied current deteriorated the degree of synchrony. Furthermore, because a finite strength of inhibitory inputs decreased the firing rates of the neurons, the boundary between the stable and the unstable antiphase states would differ from that derived by the theoretical analysis. We, however, could confirm the tendencies observed in the theoretical analysis; in-phase-preferring conductances brought a higher degree of synchrony, suggesting that such conductances promote synchronous activity of the locally connected GPe neurons. In contrast, the conductances to stabilize the antiphase state yielded a lower degree of synchrony, which lead to asynchronous activity in the network. It has been reported that the pattern of innervation from the GPe to the STN is not diverse, but selective, and that GABAergic synaptic inhibition from a single GPe neuron to an STN neuron is quite powerful (Baufreton et al. 2009). This implies that, to induce pathological rebound burst activity in the STN, global synchronization in the GPe is not necessarily required. An increase in the variability of the firing rates of GPe neurons would cause deterioration of global synchronization, as shown in Fig. 8(b2), but partial synchronization among the locally connected GPe neurons would remain a potential source of the rebound bursts in STN.

The result that the persistent sodium and potassium channels influenced the shape of the PRC is similar to that obtained in a prior analysis of a cortical fast-spiking neuron, although their contribution to synchrony differed because the kinetics of those channels and the coupling type were different (Pfeuty et al. 2003). The present study focused on the dynamics of the GPe neurons mutually connected by GABAergic synapses and assumed that GABAergic synapses were located at the soma or the proximal dendrites. The study with a multi-compartmental model of a GPe neuron revealed that excitatory inputs applied at a dendritic site could promote synchronization through the activation of dendritic SK channels (Schultheiss et al. 2010). The cooperation between somatic inhibitory inputs and dendritic excitatory inputs is an important determinant of the network behavior of GPe.

4.1 Relevance of dopaminergic modulation

Although few experimental evidences have been obtained from the GPe, dopamine can reportedly modulate some types of ionic channels, as demonstrated by experiments performed in the striatum and other regions (Surmeier et al. 2007). In the striatum, activation of the dopamine D1 receptor, D_1R, decreases the peak current through persistent sodium channels (Surmeier et al. 1992). The activation of the dopamine D2 receptor, D_2R, yields a negative shift of voltage-dependent inactivation, which presumably causes decrease in the peak current during tonic firing activity (Car et al. 2003; Surmeier et al. 1992). This evidence implies that the presence of dopamine under normal conditions should reduce the NaP current through activation of the dopamine receptors, whereas dopamine depletion under pathological conditions should enhance the NaP current. This implication and our results lead to the conclusion that dopamine depletion induces global synchrony in the GPe neurons that presumably causes rebound bursts in the STN neurons.

Dopaminergic modulation of the other ionic channels in the basal ganglia is still unclear. However, in a study with *Xenopus laevis* oocytes, dopamine D2-like receptor activation enhanced the KCNQ current (Ljungstrom et al. 2003). If dopamine has a similar effect on GPe neurons, dopaminergic modulation of more than one ionic channel should make the resulting tendency robust rather than canceling out their respective effects; a decrease in I_{NaP} and an increase in I_{KCNQ} by dopamine tended to stabilize the antiphase difference. Even if the modulation of each type of ionic channel is weak, such effects on multiple types of ionic channels could cause the transition of firing patterns (Fig. 8b1-3). As for the other neuromodulators, acetylcholine and not dopamine alters the shape of the PRC of the cortical pyramidal neurons (Stiefel et al. 2008). Similar to such cholinergic modulations, our results suggest that cellular plasticity induced by the dopamine level could trigger a transition of the neural activity patterns in the GPe network, and consequently in the STN–GPe network, from the normal tonic activity to pathological rhythmic burst activity.

Acknowledgments We thank Takeshi Takekawa for helpful comments on the numerical calculation of phase response curves.

References

Baranauskas, G., Tkatch, T., & Surmeier, D. J. (1999). Delayed rectifier current in rat globus pallidus neurons are attributable to Kv2.1 and Kv3.1/3.2 K^+ channels. *Journal of Neuroscience, 19*, 6394–6404.

Baufreton, J., Kirkham, E., Atherton, J. F., Menard, A., Magill, P. J., Bolam, J. P., et al. (2009). Sparse but selective and potent synaptic transmission from the globus pallidus to subthalamic nucleus. *Journal of Neurophysiology, 102*, 532–545.

Bevan, M. D., Wilson, C. J., Bolam, J. P., & Magill, P. J. (2000). Equilibrium potential of $GABA_A$ current and implications for

rebound burst firing in rat subthalamic neurons *in vitro*. *Journal of Neurophysiology, 83*, 3169–3172.

Bevan, M. D., Atherton, J. F., & Baufreton, J. (2006). Cellular principles underlying normal and pathological activity in the subthalamic nucleus. *Current Opinion in Neurobiology, 16*, 621–628.

Bolam, J. P., Hanley, J. J., Booth, P. A. C., & Bevan, M. D. (2000). Synaptic organisation of the basal ganglia. *Journal of Anatomy, 196*, 527–542.

Brown, P., Oliviero, A., Mazzone, P., Insola, A., Tonali, P., & Di Lazzaro, V. (2001). Dopamine dependency of oscillations between subthalamic nucleus and pallidum in Parkinson's disease. *Journal of Neuroscience, 21*, 1033–1038.

Car, D. B., Day, M., Cantrell, A. R., Held, J., Scheuer, T., Catterall, W. A., et al. (2003). Transmitter modulation of slow, activity-dependent alterations in sodium channel availability endows neurons with a novel form of cellular plasticity. *Neuron, 39*, 793–806.

Cooper, A. J., & Stanford, I. M. (2000). Electrophysiological and morphological characteristics of three subtypes of rat globus pallidus neurone *in vitro*. *Journal de Physiologie, 527*, 291–304.

DeLong, M. R., Crutcher, M. D., & Georgopoulos, A. P. (1985). Primate globus pallidus and subthalamic nucleus: functional organization. *Journal of Neurophysiology, 53*, 530–543.

Destexhe, A., Mainen, Z. F., & Sejnowski, T. J. (1998). Kinetic models of synaptic transmission. In C. Koch & I. Segev (Eds.), *Methods in neural modeling* (pp. 1–25). Cambridge: MIT.

Ermentrout, B. (1996). Type I membranes, phase resetting curves, and synchrony. *Neural Computation, 8*, 979–1001.

Ermentrout, G. B., & Kopell, N. (1984). Frequency plateaus in a chain of weakly coupled oscillators, I. *SIAM Journal on Mathematical Analysis, 15*, 215–237.

Günay, C., Edgerton, J. R., & Jaeger, D. (2008). Channel density distributions explain spiking variability in the globus pallidus: a combined physiology and computer simulation database approach. *Journal of Neuroscience, 28*, 7476–7491.

Hallworth, N. E., & Bevan, M. D. (2005). Globus pallidus neurons dynamically regulate the activity pattern of subthalamic nucleus neurons through the frequency-dependent activation of postsynaptic $GABA_A$ and $GABA_B$ receptors. *Journal of Neuroscience, 25*, 6304–6315.

Hoppensteadt, F. C., & Izhikevich, E. M. (1997). *Weakly connected neural networks*. New York: Springer.

Kita, H., & Kitai, S. T. (1994). The morphology of globus pallidus projection neurons in the rat: an intracellular staining study. *Brain Research, 636*, 308–319.

Kuramoto, Y. (1984). *Chemical oscillations, waves, and turbulence*. Berlin: Springer.

Ljungstrom, T., Grunnet, M., Jensen, B. S., & Olesen, S. P. (2003). Functional coupling between hetrologously expressed dopemine D(2) receptors and KCNQ channels. *Pflügers Archiv, 446*, 684–694.

Magill, P. J., Bolam, J. P., & Bevan, M. D. (2000). Relationship of activity in the subthalamic nucleus-globus pallidus network to cortical electroencephalogram. *Journal of Neuroscience, 20*, 820–833.

Nambu, A., & Llinás, R. (1994). Electrophysiology of globus pallidus neurons *in vitro*. *Journal of Neurophysiology, 72*, 1127–1139.

Nomura, M., Fukai, T., & Aoyagi, T. (2003). Synchrony of fast-spiking interneurons interconnected by GABAergic and electrical synapses. *Neural Computation, 15*, 2179–2198.

Pfeuty, B., Mato, G., Golomb, D., & Hansel, D. (2003). Electrical synapses and synchrony: the role of intrinsic currents. *Journal of Neuroscience, 23*, 6280–6294.

Plenz, D., & Kitai, S. T. (1999). A basal ganglia pacemaker formed by the subthalamic nucleus and external globus pallidus. *Nature, 400*, 677–682.

Raz, A., Vaadia, E., & Bergman, H. (2000). Firing patterns and correlations of spontaneous discharge of pallidal neurons in the normal and tremulous 1-methyl-4-phenyl-1,2,3,6-tetrahydropyridine vervet model of parkinsonism. *Journal of Neuroscience, 20*, 8559–8571.

Rivlin-Etzion, M., Marmor, O., Heimer, G., Raz, A., Nini, A., & Bergman, H. (2006). Basal ganglia oscillations and pathophysiology of movement disorders. *Current Opinion in Neurobiology, 16*, 629–637.

Sadek, A. R., Magill, P. J., & Bolam, J. P. (2007). A single-cell analysis of intrinsic connectivity in the rat globus pallidus. *Journal of Neuroscience, 27*, 6352–6362.

Schultheiss, N. W., Edgerton, J. R., & Jaeger, D. (2010). Phase response curve analysis of a full morphological globus pallidus neuron model reveals distinct perisomatic and dendritic modes of synaptic integration. *Journal of Neuroscience, 30*, 2767–2782.

Stanford, I. M. (2003). Independent neuronal oscillators of the rat globus pallidus. *Journal of Neurophysiology, 89*, 1713–1717.

Stiefel, K. M., Gutkin, B. S., & Sejnowski, T. J. (2008). Cholinergic neuromodulation changes phase response curve shape and type in cortical pyramidal neurons. *PLoS One, 3*, e3947.

Surmeier, D. J., Eberwine, J., Wilson, C. J., Cao, Y., Stefani, A., & Kitai, S. T. (1992). Dopamine receptor subtypes colocalize in rat striatonigral neurons. *Proc Natl Acad Sci USA, 89*, 10178–10182.

Surmeier, D. J., Ding, J., Day, M., Wang, Z., & Shen, W. (2007). D1 and D2 dopamine-receptor modulation of striatal glutamatergic signaling in striatal medium spiny neurons. *Trends in Neurosciences, 30*, 228–235.

Takekawa, T., Aoyagi, T., & Fukai, T. (2007). Synchronous and asynchronous bursting states: role of intrinsic neural dynamics. *Journal of Computational Neuroscience, 23*, 189–200.

Terman, D., Rubin, J. E., Yew, A. C., & Wilson, C. J. (2002). Activity patterns in a model for the subthalamopallidal network of the basal ganglia. *Journal of Neuroscience, 22*, 2963–2976.

Wang, X. J., & Buzsáki, G. (1996). Gamma oscillation by synaptic inhibition in a hippocampal interneuronal network model. *Journal of Neuroscience, 16*, 6402–6413.